Angular distributions and branching ratios of the electrons ejected from the Ba $[6p_{1/2\,(3/2)}ns_{1/2}]_{J=1}$ autoionizing states

R. Kachru, N. H. Tran, P. Pillet,* and T. F. Gallagher
Molecular Physics Department, SRI International, Menlo Park, California 94025
(Received 23 March 1984)

We describe the first comprehensive measurements of the energy distribution, branching ratios, and angular distributions of electrons ejected from Ba I $[6p_{1/2\,(3/2)}ns_{1/2}]_{J=1}$ states in their autoionization to the Ba II $6s$, $5d$, and $6p$ ion states. These measurements are made using a stepwise laser excitation scheme, which results in excitation of only the bound part of the autoionizing states. Furthermore, the laser excitation of these autoionizing states through the spherically symmetric Ba I $6sns\ ^1S_0$ intermediate states results in simplified electron angular distributions. We find that the Ba I $[6p_{1/2\,(3/2)}ns_{1/2}]_{J=1}$ states autoionize predominantly to an excited state of the Ba^+ ion. The interaction between the Ba I $[6p_{1/2}ns_{1/2}]_{J=1}$ and the Ba I $[6p_{3/2}ns_{1/2}]_{J=1}$ series manifests itself in the sharp variation in the electron asymmetry parameter β near the neighborhood of the interaction. We also present a simple analysis of our results incorporating the multichannel quantum-defect theory.

I. INTRODUCTION

For the last few years the spectroscopy of He-like alkaline-earth atoms—Mg, Ca, Sr, and Ba—has attracted considerable interest. For example, the selective, stepwise excitation of the high-lying bound Rydberg states of alkaline-earth atoms has led to a precise measurement of the level positions of many states.[1–6] Typically, the two-electron spectra are more complex than the single-valence-electron alkali-metal atoms because each Rydberg series is perturbed by states converging to the same or other ionization limits. Nonetheless, the resulting spectra have been successfully modeled using multichannel quantum-defect theory (MQDT).[7–10] While the bound part of the spectrum is fairly well understood, the same is not true for the autoionizing states.

Autoionizing states of atoms are those states for which the sum of the energy of the excited electrons exceeds the energy required to ionize at least one electron of the atom. These states have inherently short lifetimes and decay by ejecting an electron, leaving the ion in its ground state or in an excited state. There have been very few systematic studies of the autoionizing states which lie above the first ionization threshold. The positions and widths of some autoionizing Rydberg series of Ba and Sr have been reported.[11–16] For example, the width of an autoionizing resonance gives the total autoionization rate, but does not provide any information about the final states of the ion core. The knowledge of autoionization rates or the branching ratio to a particular ion state is important in many physical problems. For example, it is important to know if the autoionization leads to the ion core in the ground or excited state in such diverse problems as an autoionization laser[17] or the energy loss due to dielectronic recombination in plasmas. Moreover, the knowledge of autoionization rates is of fundamental importance in any calculation of wave functions in the autoionization region.

Originally, autoionizing levels were studied using photoexcitation from the ground state with ultraviolet light.[18,19] Usually under these conditions the excitation line shape is an asymmetric Beutler-Fano profile,[20] which results from the interference between the excitation to the bound and to the continuum part of the autoionization state, respectively. By exciting an autoionizing state, stepwise through bound states, with use of tunable dye lasers, a symmetric Lorentzian excitation line profile is obtained. This is because the excitation cross section to the continuum part of the autoionization state, from the bound Rydberg state, is considerably smaller than that to the bound part.[21,22] The stepwise excitation scheme not only simplifies the analysis of the autoionization spectrum but also requires very modest laser power, since all the laser-driven transitions are single-electron transitions (see below).

Before we describe our present measurements in detail, let us digress briefly on the specific system under study, the Ba I $[6p_{1/2\,(3/2)}ns_{1/2}]_{J=1}$ states. As shown in Fig. 1, we excite to the Ba I $[6p_{1/2}20s_{1/2}]_{J=1}$ state, for instance, from the Ba I ground $6s^2\ ^1S_0$ state via the $6s6p\ ^1P_0$ and $6s20s\ ^1S_0$ states, using three dye lasers which drive these transitions resonantly. Degenerate with the Ba I $[6p_{1/2}ns_{1/2}]_{J=1}$ state to which we excite are Ba I $6s_{1/2}\epsilon p_{1/2\,(3/2)}$ and $5d_{3/2\,(5/2)}\epsilon p,\epsilon f$ continua with odd parity and $J=1$. The autoionization thus leads to either a Ba II $6s_{1/2}$ or $5d_{3/2\,(5/2)}$ ion along with an ejected electron with 2.6 or 1.9 eV of energy, respectively. It is interesting to note that we excite to the Ba I $[6p_{1/2\,(3/2)}ns_{1/2}]_{J=1}$ states from the spherically symmetric Ba I $6sns\ ^1S_0$ state with the third laser. Thus we have a dipole excitation of an unaligned system, and Yang's theorem[23] may be applied to predict the form of the electron angular distribution. This problem is, of course, similar to that of photoexcitation from a $^1S_0$ ground state.

Recently we reported the energy and angular distribution measurements of the electrons ejected from the Ba I $[6p_{1/2\,(3/2)}ns_{1/2}]_{J=1}$ states.[24] From these measurements we inferred the branching ratios to the Ba II $6s$, $5d$, and

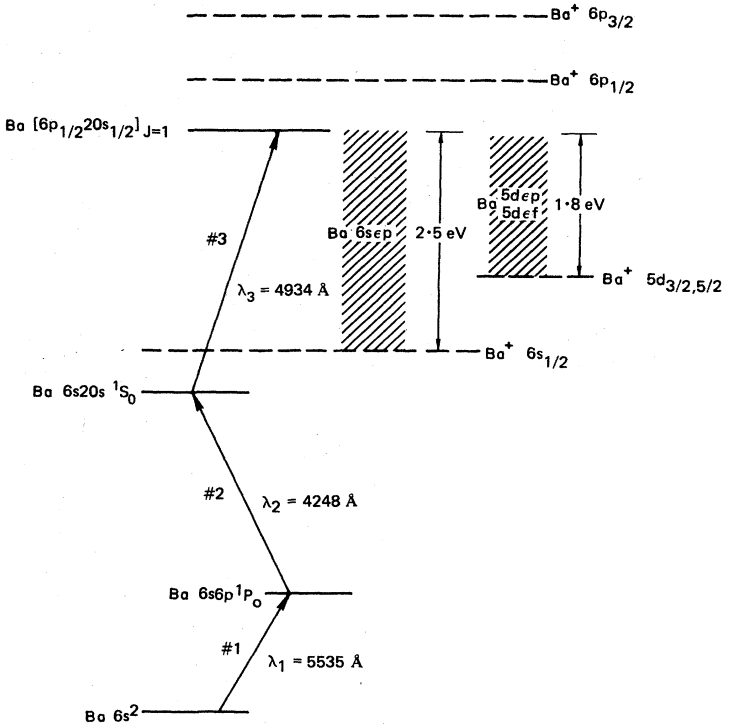

FIG. 1. Simplified energy-level diagram of Ba relevant to our experiment. The Ba I $[6p_{1/2\,(3/2)}ns_{1/2}]_{J=1}$ states are stepwise excited by three tunable dye laser pulses. Degenerate with the Ba I $[6p_{1/2}20s_{1/2}]_{J=1}$ state shown here are the Ba I $6s\epsilon p$, $5d\epsilon p$, and $5d\epsilon f$ continua. The dashed lines represent the Ba^+-ion energy levels as indicated. The first two dye lasers resonantly excite the Ba atoms from the $6s^2\,{}^1S_0$ ground state to the $6sns\ {}^1S_0$ Rydberg state via the $6s\,6p\ {}^1P_0$ level. The Ba I $[6p_{1/2\,(3/2)}ns_{1/2}]_{J=1}$ states are excited from the spherically symmetric Ba I $6sns\ {}^1S_0$ state with the third laser.

$6p_{1/2}$ states. Together with the previous measurements of the total ionization rates, these data yield the autoionization rates to each particular final ion state.

In this paper we present results which extend our previous measurements and also provide details of autoionization branching ratios which were unresolved in our previous study. We also present a more detailed account of our experimental approach and observations as well as a simple analysis of our results.

In Sec. II we describe the experimental approach. The measurements of the autoionization branching ratios and electron angular distributions are discussed in Sec. III. We also discuss some of the salient features emerging from our measurements, particularly those involving the electron angular distributions. In Sec. IV we develop a simple model of the autoionization process based on the MQDT.

II. EXPERIMENT

The experimental arrangement used for measuring the electron energy and angular distribution is shown in Fig. 2. An effusive Ba beam, produced by a resistively heated oven, passes between two parallel plates separated by 1.0 cm. The lower plate is typically grounded while a voltage may be applied to the upper plate to produce any desired electric field in the interaction region. The three tunable laser pulses required in this experiment are produced by three dye lasers of Hänsch design pumped by the harmonics of a Quanta Ray Nd^{3+}:yttrium-aluminum-garnet (YAG) laser operating at 10 Hz. The dye laser pulses, with 10 GHz linewidth full width at half maximum (FWHM), have typical energies of ~ 100 μJ per pulse. The first dye laser pumps the Ba I $6s^2$-$6s\,6p$ ($\lambda = 5535$ Å) transition while the second dye laser pumps the Ba I $6s\,6p$-$6sns$ ($\lambda \sim 4250$ Å) transition. A 5-ns delay in the second dye laser beam ensures that when it arrives in the interaction region the Ba I $6s\,6p$ state is populated. The third dye laser ($\lambda \sim 4934$ or 4554 Å) excites the spherically symmetric Ba I $6sns\ {}^1S_0$ state to the autoionizing Ba I $[6p_{1/2\,(3/2)}ns_{1/2}]_{J=1}$ state. The three dye laser beams propagating almost collinearly pass through a linear polarizer and cross the Ba beam at right angles near the center of the plates.

The electrons ejected from the Ba I $[6p_{1/2\,(3/2)}ns_{1/2}]_{J=1}$ autoionizing state quickly move out of the interaction region through a 1-mm-wide slot in the lower plate into the electron energy analyzer. The 127° electrostatic energy analyzer is designed to operate in the 0—10-eV range and has an energy resolution $\Delta E/E$ of 5%. The entire interaction region along with the energy analyzer is enclosed by a magnetic shield to reduce the magnetic field to ~ 1 mG.

Since the analyzer is fixed in its positions, the angular distribution of the ejected electrons is obtained by changing the angle between the polarization of the incident dye laser beams relative to the input axis of the analyzer. This

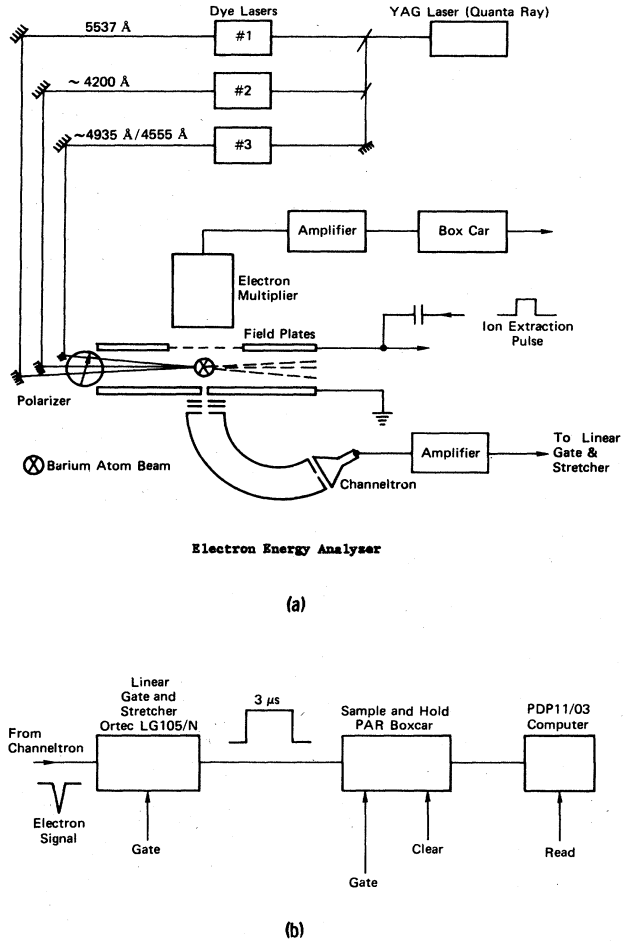

FIG. 2. (a) Schematic of experimental apparatus. Pumped by the harmonics of a single Quanta Ray Nd^{3+}:YAG laser, dye lasers DL1—DL3 are tuned to the Ba $6s^2\,{}^1S_0$—$6s\,6p\,{}^1P_0$, $6s\,6p\,{}^1P_0$—$6sns\,{}^1S_0$, and $6sns\,{}^1S_0$—$[6p_{1/2\,(3/2)}ns_{1/2}]_{J=1}$ transitions (see Fig. 1), respectively. The three dye laser beams travel almost collinearly and pass through a linear polarizer before crossing the Ba beam at right angles near the center of the field plates. The electrons ejected from the autoionizing states quickly pass through the 1-mm slot in the center of the lower plate into the 127° electrostatic energy analyzer. The electron angular distributions are obtained by changing the polarization direction of the three laser beams relative to the fixed energy analyzer by rotating the polarizer. Both the ejected electrons and the ions are detected in this experiment. The electrons emerging from the energy analyzer are detected by a channeltron. A 0.3-μs-risetime—100-V pulse applied to the upper place pushes the ion through a grid into an EMI electron multiplier. The signal from the channeltron and the electron multiplier is amplified by a fast amplifier before being processed. (b) Schematic of data-acquisition system. The amplified electron signal of a few nanoseconds width is integrated by an EG&G LG105/N linear gate and stretcher, which provides a 3-μs-long output pulse. A PAR model-162 boxcar used as a sample-and-hold circuit holds the output of the stretcher until it is read by the DEC PDP11/03 microcomputer via an analog-to-digital converter. The ion signal is integrated by another channel of the boxcar and read by the computer. The electron and ion signals are recorded after every laser shot (typically 10 Hz).

is achieved by rotating the polarization axis of the linear polarizer as shown in Fig. 2(a). The energy spectrum of the electrons is determined by accelerating or decelerating the electrons as they traverse the apertures in front of the analyzer so as to match the analyzer transmission energy which is kept fixed. The acceptance azimuthal angle of the analyzer, primarily defined by the apertures in front of it, is $\sim 1°$. In the present work the analyzer transmission energy is typically kept at 8 eV which provides a good "throughput," albeit at low resolution ($\Delta E \sim 0.4$ eV). For the high-resolution measurements the transmission energy is 1 eV ($\Delta E \sim 0.05$ eV). The electrons are detected by a channel electron multiplier which is placed near the exit slits of the energy analyzer.

We measure the angular distribution of the electrons to a specific state of the Ba^+ ion (corresponding to a specific fixed energy of the ejected electrons) by rotating the polarization of the lasers and recording the electron signal at a fixed electron energy. The rotation of the polarizer leads to some variation (typically $\pm 15\%$ over the full 360° rotation) in the laser intensity of the beams and hence in the number of barium atoms excited to the specific autoionizing state. A convenient way to circumvent this problem is to normalize the electron signal by the total number of ions produced. The ions are collected by applying a 100-V pulse to the upper plate 0.5 μs subsequent to the laser pulses. This pulls the ions through the grid in the upper plate into a particle multiplier (EMI 9642). The ion signal from the particle multiplier is amplified and fed into a Princeton Applied Research (PAR) boxcar averager which is used in the sample and hold mode. The electron signal from the channeltron is typically amplified in voltage by 100 and fed into a gated pulse stretcher (EG&G LG105/N) whose output is fed into the boxcar and subsequently read by a Digital Equipment Corporation (DEC) PDP11/03 microcomputer [see Fig. 2(b)]. Finally, the electron and ion signals are averaged by the computer over 20—100 laser shots.

The three dye laser beams are loosely focused and have a diameter of 1 mm in the interaction region where the Ba number density is 10^9 atoms/cm^3. Since the autoionizing linewidth is typically larger than the dye laser linewidth the third dye laser is always tuned to the center of the autoionization resonance in all our measurements. However, in a subsidiary experiment the electron β parameter (see below) and the autoionization branching ratios to the various Ba^+ states are measured as the frequency of the third laser is swept across the line profile of a few Ba I $[6p_{1/2\,(3/2)}ns_{1/2}]_{J=1}$ states. It is worthwhile to recall that in some previous experiments involving photoexcitation from the ground state, the asymmetry parameter varies dramatically with photoexcitation energy in the vicinity of autoionizing states.[25] The variation in the asymmetry parameter or the ion branching ratio in these previous experiments is a manifestation of the interference between the photoexcitation to the discrete autoionization state and to the underlying continuum.

III. RESULTS AND DISCUSSION

One of the primary objectives of the present work is to determine the autoionization branching ratios of the Ba I

$[6p_{1/2\,(3/2)}ns_{1/2}]_{J=1}$ states to all the allowed states of the Ba^+ ion and ejected electron. Since the ions that result from autoionization provide no information about their electronic state in this experiment, we analyze the energy of the ejected electrons instead to determine the final state. Specifically, energy conservation results in a one-to-one correspondence between the energy of the ejected electron and the final state of the ion. Of course, the degenerate states of either the ion or the ejected electron cannot be distinguished in this manner. In measuring the autoionization branching ratios by counting the number of ejected electrons of a particular energy, we have to remember that the electrons are not necessarily ejected isotropically. It is therefore necessary to measure their angular distributions. From the angular distribution, the total number of ejected electrons of a given energy integrated over all angles can be computed. This number is the autoionization rate to a specific final ion state. In our experiment we do not directly measure the absolute autoionization rates to the various ion states. From the energy analysis and angular distribution of the electrons we determine the relative rates, i.e., the branching ratios. Also, the observed width of the autoionizing states is equal to the sum of the autoionization rates to all allowed states of the rsulting ion and ejected electrons. Thus, from the knowledge of the electron branching ratios and the width of the Ba I $[6p_{1/2\,(3/2)}ns_{1/2}]_{J=1}$ state, the absolute autoionization rate to any final state of the ion and ejected electron can be computed.

The first step in the process to measure electron angular distribution is to identify the final ion states to which any given autoionizing state can decay. Figure 3 shows a scan of the signal obtained from the energy analyzer corresponding to the autoionization of the Ba I $[6p_{3/2}15s_{1/2}]_{J=1}$ state. The upper and lower traces correspond to $\theta=90°$ and 0°, respectively, where θ is the angle between the analyzer and the polarization direction. The first peak of the lower trace corresponds to the decay of the initial state to the Ba II $6s_{1/2}$ state of the ion and ejection of a 2.6-eV electron (see Fig. 1 for the energy-level diagrams for the relevant states). The 2.6-eV electron peak for $\theta=90°$ (upper trace) appears to be missing because it is very small compared with the other peaks shown in Fig. 3. The second and third peaks in Fig. 3 (on both upper and lower traces) are electrons ejected with energies of 1.9 and 0.1 eV, respectively. As can be seen from Fig. 1 these electron energies correspond to autoionization of the Ba I $[6p_{3/2}15s_{1/2}]_{J=1}$ state to the Ba II $5d_{3/2\,(5/2)}$ and $6p_{1/2}$ states of the ion, respectively. As noted before, in the present measurements the transmission energy of the analyzer is fixed at either 8 or 1 eV. While the low transmission energy of 1 eV provides an energy resolution of $\Delta E/E$ of $\sim$0.05 eV, sufficient to resolve the fine structure of the Ba II $5d$ ion state, it also results in a sharply reduced analyzer throughput. We use the analyzer transmission energy of 1 eV only in those measurements where we attempt to resolve the 0.09-eV fine structure of Ba II $5d$ ion state. In Fig. 3 the fine structure of the Ba II $5d$ state is unresolved.

A typical electron angular distribution obtained for a fixed electron energy is shown in Fig. 4. The plot in Fig.

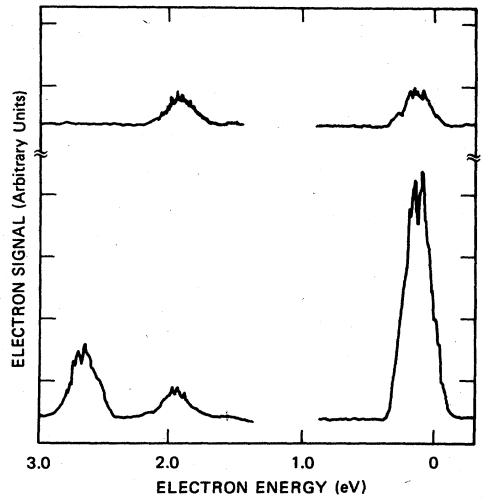

FIG. 3. Typical electron signal from the energy analyzer. The upper and lower traces correspond to $\theta=90°$ and 0°, respectively, where θ is the angle between the analyzer and the laser polarization direction. The peaks seen on the upper and lower traces correspond to the autoionization of the Ba $[6p_{3/2}15s_{1/2}]_{J=1}$ state to the Ba II $6s_{1/2}$, $5d$, and $6p_{1/2}$ states and ejection of 2.6-, 1.9-, and 0.1-eV electrons, respectively. Note that the 2.6-eV electron peak for $\theta=90°$ (upper trace) appears to be missing because it is very small compared to the other peaks. In obtaining these traces, the transmission energy of the electron energy analyzer is kept fixed at 8 eV, while the electrons are accelerated before entering the input slit. Note that the Ba II $5d_{5/2}$ and $5d_{3/2}$ states are unresolved in this trace.

4 shows the angular distribution of the 2.6-eV electrons ejected from the autoionizing Ba I $[6p_{3/2}20s_{1/2}]_{J=1}$ state. The final ion state associated with 2.6-eV electrons is Ba II $6s_{1/2}$. Each point in this plot represents an average of the normalized electron signal (the electron signal divided by the total ion signal) over 75 laser shots. The broken curve

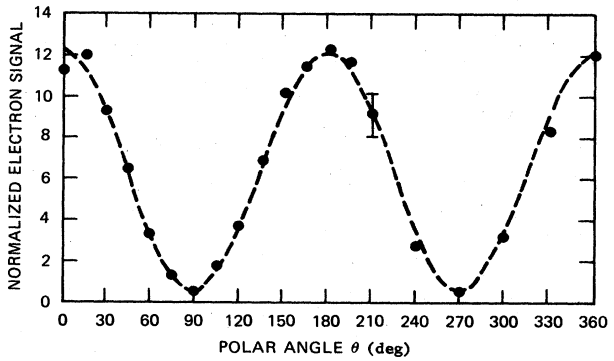

FIG. 4. Angular distribution of the 2.6-eV electron ejected from the autoionization of the Ba I $[6p_{3/2}20s_{1/2}]_{J=1}$ state to the Ba II $6s_{1/2}$ state of the ion. The dots are the experimental points obtained by measuring the 2.6-eV electron signal and dividing by the ion's signal and averaging it over 75 laser shots with the computer (see text). The angle θ is changed by rotating the polarizer, which varies the angle between the fixed electron energy analyzer (acceptance angle $\sim$1°) and the laser polarization direction. The dashed line is a best fit to Eq. (1).

is the best fit to the curve $I(\theta)=(I_0/4\pi)[1+\beta P_2(\cos\theta)]$, where $I(\theta)$ is the electron signal at angle θ, $P_2(\cos\theta)$ is the Legendre polynomial of order 2, and β is a constant. The agreement between the observed data and the fit is quite good. In fact, all our electron angular distribution data can be fitted quite well with the equation

$$I(\theta)=\frac{I_0(nl_j)}{4\pi}[1+\beta(nl_j)P_2(\cos\theta)]\ , \tag{1}$$

where $\beta(nl_j)$ is a constant (for a fixed final ion state), commonly referred to as the asymmetry parameter, and nl_j refers to the Ba II $6s_{1/2}$, $5d_{3/2\,(5/2)}$, or $6p_{1/2}$ state of the ion.

As stated earlier, in our experiment the excitation to the autoionizing Ba I $[6p_{1/2\,(3/2)}ns_{1/2}]_{J=1}$ state starts from an unpolarized Ba I $6sns\ ^1S_0$ state. Assuming electric dipole excitation to the autoionizing state, Yang's theorem[23] predicts an angular distribution which is of the form expressed in Eq. (1). We fit all our angular distribution data to Eq. (1) and determine the parameters I_0 and β. Since I_0 is proportional to the total number of electrons ejected over all angles for a given final state of the ion, the branching ratios for autoionization of the Ba I $[6p_{1/2\,(3/2)}ns_{1/2}]_{J=1}$ state to various final ion states can now be computed quite easily. Consider, for example, the autoionization of the Ba I $[6p_{1/2}9s_{1/2}]_{J=1}$ state. Ignoring the fine structure of the Ba II $5d$ ion state the autoionization channels can be written as

$$\mathrm{Ba}([6p_{1/2}9s_{1/2}]_{J=1})\rightarrow \mathrm{Ba\ II}(6s)+e^-(\epsilon l\ (\epsilon=2.0\ \mathrm{eV}))\ , \tag{2a}$$

$$\mathrm{Ba}([6p_{1/2}9s_{1/2}]_{J=1})\rightarrow \mathrm{Ba\ II}(5d)+e^-(\epsilon l\ (\epsilon=1.3\ \mathrm{eV}))\ , \tag{2b}$$

where ϵ and l are the ejected-electron energy and orbital angular momentum, respectively. The measured angular distributions of the 2.0- and 1.3-eV electrons, respectively, are shown in Figs. 5(a) and 5(b). The solid line, as before, is the best fit to the measured distribution, shown as dots. While the asymmetry parameter for the 2.0-eV electrons β(Ba II $6s_{1/2}$) [Eq. 2(a)] is 1.4, the angular distribution for the 1.3-eV electrons [Eq. 2(b)] is almost isotropic, with β(Ba II $5d$)=0.1. From the fit we also obtain for I_0 the values 49 and 33 for the plots shown in Figs. 5(a) and 5(b), respectively. This gives a branching ratio I_0(Ba II $6s_{1/2}$)/[I_0(Ba II $6s_{1/2}$)+I_0(Ba II $5d$)]=60% and I_0(Ba II $5d$)/[I_0(Ba II $6s_{1/2}$)+I_0(Ba II $5d$)]=40%.

Before we discuss the values of the asymmetry parameter and the autoionization branching ratios for the Ba I $[6p_{1/2\,(3/2)}ns_{1/2}]_{J=1}$ series in detail, it is important to mention the result of a subsidiary experiment mentioned earlier. Specifically, in this experiment we measure the asymmetry parameter and the autoionization branching ratios for a few selected Ba I $[6p_{1/2\,(3/2)}ns_{1/2}]_{J=1}$ states, as the frequency of the third laser is scanned across the line profile of these autoionizing states. Within the limits of our experimental error we do not find any variation in the β parameter or the autoionization branching ratios as the frequency of the third dye laser is swept across the excitation line profile of the selected isolated Ba I $[6p_{1/2\,(3/2)}ns_{1/2}]_{J=1}$ autoionizing states. This observation simplifies the experiment as well as its interpretation. Furthermore, this observation is to be contrasted with previous experiments involving photoexcitation of atoms from the ground state. In these experiments, photoelectron angular distributions show pronounced variation as a function of photon energy, as it is swept across the autoionizing resonance. Since in our excitation scheme the autoionizing states are excited from a Rydberg state, the excitation cross section to the continuum is at least a factor of 10^3 smaller compared with the excitation cross section to the bound part of the autoionizing state.[21,22] It is therefore hardly surprising to see no variation in the β parameter and the autoionization branching ratio with energy.

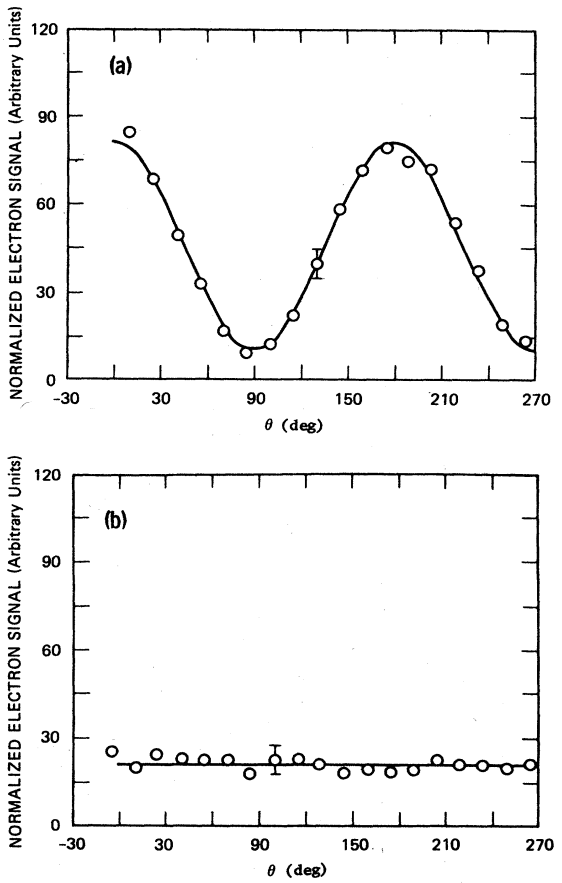

FIG. 5. (a) The measured normalized electron angular distributions of the 2.0-eV electrons ejected from the autoionization of the Ba I $[6p_{1/2}9s_{1/2}]_{J=1}$ state [see Eq. (2a)]. The final Ba-ion state in this case is Ba II $6s_{1/2}$. The dashed line is the best fit to Eq. (1), with β(Ba II $6s_{1/2}$)=1.4. (b) Angular distribution of 1.3-eV electrons ejected from the autoionization of the Ba I $[6p_{1/2}9s_{1/2}]_{J=1}$ state [see Eq. (2b)]. Note that the electron angular distribution is almost isotropic with β(Ba II $5d$)=0.1.

The branching ratios for the Ba I $[6p_{1/2}ns_{1/2}]_{J=1}$ states autoionizing to the Ba II $6s$ ground and $5d$ excited states of the ion are listed in Table I and are plotted as a function of n in Fig. 6. The asymmetry parameter β for the

TABLE I. Branching ratios for the Ba $[6p_{1/2}ns_{1/2}]_{J=1}$ autoionizing states leading to the $6s_{1/2}$ ground and $5d_{5/2(3/2)}$ excited states of Ba II. The errors shown in parentheses represent the statistical uncertainty in our data.

Ba I autoionizing state	Branching ratio to Ba^+-ion state (%)	
	Ba II $6s_{1/2}$	Ba II $5d_{3/2\,(5/2)}$
$6p_{1/2}9s_{1/2}$	65(10)	35
$6p_{1/2}12s_{1/2}$	24(5)	76
$6p_{1/2}13s_{1/2}$	25(5)	75
$6p_{1/2}14s_{1/2}$	9(5)	91
$6p_{1/2}15s_{1/2}$	38(5)	62
$6p_{1/2}16s_{1/2}$	17(5)	83
$6p_{1/2}17s_{1/2}$	20(5)	80
$6p_{1/2}19s_{1/2}$	23(5)	77
$6p_{1/2}20s_{1/2}$	16(5)	84
$6p_{1/2}21s_{1/2}$	10(5)	90
$6p_{1/2}22s_{1/2}$	15(5)	85
$6p_{1/2}23s_{1/2}$	37(5)	63
$6p_{1/2}25s_{1/2}$	44(8)	56

ejected electrons leading to either the Ba II $6s$ or $5d$ state of the ion are listed in Table II and plotted in Fig. 7. The electron asymmetry parameter β(Ba II $6s_{1/2}$) leading to the Ba II $6s_{1/2}$ final ion state is shown plotted in Fig. 7 as open circles, while β(Ba II $5d$) is plotted as open squares.

The large fine-structure splitting (1691 cm^{-1}) of the Ba II $6p$ state of the ion leads to Ba I $[6p_{3/2}ns_{1/2}]_{J=1}$ levels with $n \geq 12$ being energetically above the Ba II $6p_{1/2}$ ion state. This opens another autoionization channel for the Ba I $[6p_{3/2}ns_{1/2}]_{J=1}$ levels with $n \geq 12$. The branching ratios for the autoionization of Ba I $[6p_{3/2}ns_{1/2}]_{J=1}$ states to the Ba II $6s_{1/2}$, $5d$, and $6p_{1/2}$ ion states are tabulated in Table III, while the electron asymmetry parameter β for each decay channel is listed in Table IV.

In Fig. 8 the branching ratios for autoionization to the Ba II $6s_{1/2}$, $5d$, and $6p_{1/2}$ ion states are plotted as a function of n, while β(Ba II $6s_{1/2}$), β(Ba II $5d$), and β(Ba II $6p_{1/2}$) are plotted in Fig. 9. It is worth noting that in the measurements tabulated in Tables I–IV and Figs. 6–9 we have not attempted to resolve the two possible Ba II $5d$ fine-structure states of the ion. In these measurements for branching ratios to the Ba II $5d$ ion state, we are in fact performing an incoherent sum over the $j=\frac{3}{2}$ and $\frac{5}{2}$ ion states, while the measurements for β reflect an incoherent average over the fine-structure states. Obviously, for a complete understanding of the autoionization process the knowledge of the autoionization rate and the electron β parameter for each final ion state is required. However, as we shall see, the number of parameters required to fit all the data to the theory incorporating MQDT for all sets of final Ba II $5d$ fine-structure states is quite large. We have therefore taken most of our data without resolving

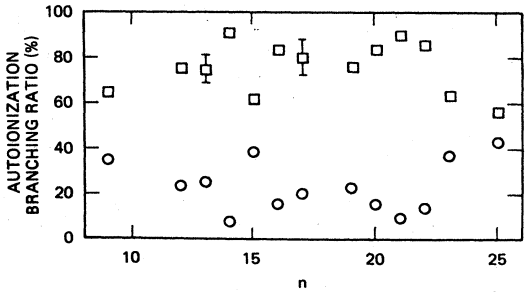

FIG. 6. Branching ratios for the Ba $[6p_{1/2}ns_{1/2}]_{J=1}$ autoionizing states to the Ba II $6s_{1/2}$ state (open circles) and Ba II $5d$ state (open squares) plotted as a function of n. The errors shown are typical and represent the statistical error in our data. The autoionization branching ratios to the two possible $5d$ fine-structure states of Ba II are unresolved in these measurements.

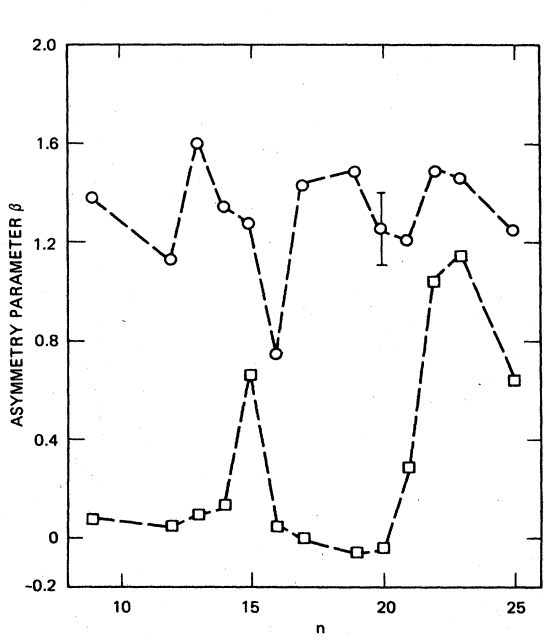

FIG. 7. Ejected-electron asymmetry parameter of the Ba I $[6p_{1/2}ns_{1/2}]_{J=1}$ states β(Ba II $6s_{1/2}$) (open circles) and β(Ba II $5d$) (open squares) plotted as a function of n. The errors shown are typical and represent the statistical error in these measurements. The dashed line connects the successive data points. Note that in the measurements of β(Ba II $5d$) the two possible Ba II $5d$ fine-structure states of the ion remain unresolved. The measured value of β(Ba II $5d$) therefore is an incoherent average of β(Ba II $5d_{3/2}$) and β(Ba II $5d_{5/2}$) (see text).

TABLE II. The ejected-electron asymmetry parameters β(Ba II $6s_{1/2}$) and β(Ba II $5d$) for the Ba I $[6p_{1/2}ns_{1/2}]_{J=1}$ autoionizing state.

Ba I autoionizing state	Electron asymmetry parameter β(Ba II $6s_{1/2}$)	β(Ba II $5d$)
$6p_{1/2}9s_{1/2}$	1.38(15)	0.08(15)
$6p_{1/2}12s_{1/2}$	1.14(10)	0.05(10)
$6p_{1/2}13s_{1/2}$	1.67(15)	0.01(10)
$6p_{1/2}14s_{1/2}$	1.34(15)	0.13(10)
$6p_{1/2}15s_{1/2}$	1.28(10)	0.72(10)
$6p_{1/2}16s_{1/2}$	0.71(10)	0.06(10)
$6p_{1/2}17s_{1/2}$	1.44(15)	−0.01(10)
$6p_{1/2}19s_{1/2}$	1.49(15)	−0.06(10)
$6p_{1/2}20s_{1/2}$	1.25(15)	−0.04(10)
$6p_{1/2}21s_{1/2}$	1.21(15)	0.28(15)
$6p_{1/2}22s_{1/2}$	1.5(2)	1.05(20)
$6p_{1/2}23s_{1/2}$	1.46(15)	1.16(15)
$6p_{1/2}25s_{1/2}$	1.25(15)	0.65(15)

the Ba II $5d$ ion fine-structure states, as the signal obtained through the analyzer at high resolution is small and the statistical uncertainty in the data is large. However, for completeness, we have recorded the branching ratios and β parameters for a few Ba I $[6p_{1/2\,(3/2)}ns_{1/2}]_{J=1}$ states in which the Ba II $5d_{3/2}$ and $5d_{5/2}$ final ion states are completely resolved (see below).

The n dependence of the branching ratios for the Ba I $[6p_{3/2}ns_{1/2}]_{J=1}$ series autoionizing to the Ba II $6s_{1/2}$ or $5d$ ion state, as can be seen from Fig. 8 or Table III, does not show much variation. The branching ratio I_0(Ba II $6s_{1/2}$)/[I_0(Ba II $6s_{1/2}$)+I_0(Ba II $5d$)] is approximately 40% for all n states except $n=9$, which has a somewhat higher value of 65%. The value of β remains almost constant as a function of n (see Fig. 9), except for a gradual increase in β(Ba II $5d$) at high n ($n=24$ and 25). It is also interesting to note the difference in the electron angular distribution associated with the Ba II $6s_{1/2}$ and $5d$ final ion state. While β(Ba II $5d$)$\sim$0.2–0.3 reflects an almost isotropic angular distribution, the electrons associated with the ion returning to the Ba II $6s_{1/2}$ ground state are ejected very anisotropically with an angular distribution which is almost purely $\sim\cos^2\theta$ [β(Ba II $6s_{1/2}$)$\simeq$1.8)] [see Eq. (1)].

Another interesting aspect of the branching-ratio measurements is that about 65–70% of the total autoionization of the Ba I $[6p_{3/2}ns_{1/2}]_{J=1}$ states is to the Ba II $6p_{1/2}$ state of the ion (see Table III). The large autoionization rate to the Ba II $6p_{1/2}$ state of the ion, also inferred from purely spectroscopic measurements, has led recently to the development of a Ba^+ laser.[17] Equally intriguing is the large asymmetry parameter β(Ba II $6p_{1/2}$)$\sim$1.5 (see Table IV) for the ejected electrons. If this autoionization proceeds purely via the $1/r_{12}$ Coulomb repulsion of the two electrons then in the independent-electron model, this must proceed via the quadrupolar term in the $1/r_{12}$ expansion, which would necessarily lead to only ϵd electrons. This, as we shall see later, should result in $\beta=1$, which seems to be in contradiction to the observed value of β(Ba II $6p_{1/2}$)$\simeq$1.5.

While the n dependence of branching ratios and β parameters to the various ion states for the Ba I $6p_{3/2}ns$ series is fairly constant, similar measurement on the Ba I $6p_{1/2}ns_{1/2}$ series shows sharp irregularities. For instance, as shown in Fig. 6 and Table I, the branching ratios to the Ba II $6s$ and $5d$ states of the ion show structure near $n=15$ and 24. Similarly, Fig. 7 shows structure in the plot of β(Ba II $6s$) and β(Ba II $5d$) versus n near $n=15$

TABLE III. Branching ratios for the Ba $[6p_{3/2}ns_{1/2}]_{J=1}$ autoionizing states leading to the $6s_{1/2}$, $5d$, and $6p_{1/2}$ states of Ba II.

Ba I autoionizing state	Branching ratios to the Ba^+-ion state (%) Ba II $6s_{1/2}$	Ba II $5d_{5/2\,(3/2)}$	Ba II $6p_{1/2}$
$6p_{3/2}9s_{1/2}$	65(8)	35(8)	
$6p_{3/2}14s_{1/2}$	9(3)	12(4)	79
$6p_{3/2}15s_{1/2}$	12(3)	15(3)	73
$6p_{3/2}16s_{1/2}$	11(3)	16(3)	73
$6p_{3/2}17s_{1/2}$	11(3)	17(3)	72
$6p_{3/2}19s_{1/2}$	11(3)	17(3)	72
$6p_{3/2}20s_{1/2}$	11(3)	27(3)	62
$6p_{3/2}21s_{1/2}$	14(3)	21(3)	65
$6p_{3/2}22s_{1/2}$	12(3)	18(3)	70
$6p_{3/2}24s_{1/2}$	14(3)	21(3)	65
$6p_{3/2}25s_{1/2}$	14(3)	21(3)	65

TABLE IV. The ejected-electron asymmetry parameters β(Ba II $6s_{1/2}$), β(Ba II $5d$), and β(Ba II $6p_{1/2}$) for the Ba I $[6p_{3/2}ns_{1/2}]_{J=1}$ autoionizing states.

Ba I autoionizing state	Electron asymmetry parameter β(Ba II $6s_{1/2}$)	β(Ba II $5d$)	β(Ba II $6p_{1/2}$)
$6p_{3/2}9s_{1/2}$	1.85(20)	−0.1(2)	
$6p_{3/2}14s_{1/2}$	1.7(2)	0.14(20)	1.6(2)
$6p_{3/2}15s_{1/2}$	1.7(2)	0.25(20)	1.55(15)
$6p_{3/2}16s_{1/2}$	1.85(25)	0.2(2)	1.6(2)
$6p_{3/2}17s_{1/2}$	1.8(2)	0.3(2)	1.6(2)
$6p_{3/2}19s_{1/2}$	1.8(2)	0.22(20)	1.6(2)
$6p_{3/2}20s_{1/2}$	1.74(20)	0.4(2)	1.5(2)
$6p_{3/2}21s_{1/2}$	1.67(20)	0.4(2)	1.5(2)
$6p_{3/2}22s_{1/2}$	1.74(20)	0.45(20)	1.55(20)
$6p_{3/2}24s_{1/2}$	1.61(20)	0.54(20)	1.55(20)
$6p_{3/2}25s_{1/2}$	1.65(20)	0.8(3)	1.55(20)

and 24. From the spectroscopic measurements of Bhatti and Cooke[15] it is clear that the Ba I $[6p_{1/2}ns_{1/2}]_{J=1}$ series interacts with the Ba I $[6p_{3/2}ns_{1/2}]_{J=1}$ series near $n=15$ and 24. This is also seen clearly in Fig. 10, which is the Lu-Fano plot[26] of $\nu_{1/2}$ (modulo 1) versus $\nu_{3/2}$ (modulo 1), where $\nu_{1/2\,(3/2)}$ are the effective quantum numbers of the Ba I $[6p_{1/2}ns_{1/2}]_{J=1}$ series relative to the Ba I $6p_{1/2}$ and $6p_{3/2}$ ionization limits, respectively. Specifically, the Lu-Fano plot shows that the effective quantum number $\nu_{1/2}$ (modulo 1) has a significant departure from its constant value in the vicinity of $n=15$ and 24. This perturbation in the value of $\nu_{1/2}$ (modulo 1) is caused by the interaction of Ba I $[6p_{1/2}15s_{1/2}]_{J=1}$ levels with the degenerate Ba I $[6p_{3/2}11s_{1/2}]_{J=1}$ level belonging to the Ba I $6p_{3/2}$ series. Moreover, this interaction also leads to mixing between levels of the two series. We also note that a similar interaction between the Ba I $[6p_{1/2}nd_{3/2\,(5/2)}]_{J=3}$ series with Ba I $[6p_{3/2}n'd_{3/2\,(5/2)}]_{J=3}$ levels occurs near $n'=10$. This was recently investigated by Gounand *et al.*, who were also successful in analyzing this interaction in terms of a few MQDT parameters.[14]

Returning to Fig. 7, we see that the sharp variation in the β parameter and the branching ratios in the vicinity of $n=15$ and 24 is caused by the mixing of Ba I $[6p_{1/2}ns_{1/2}]_{J=1}$ states with Ba I $[6p_{3/2}n's_{1/2}]_{J=1}$ levels ($n'=11$ and 12). Ignoring for the moment the variation of β and the branching ratios in the vicinity of the perturbation at $n=15$ and 25, we observe from Fig. 6 that the autoionization rate to the Ba II $5d$ ion state is a factor of 3 larger than that to the Ba II $6s$ state. The electron asymmetry parameter β(Ba II $5d$), as can be seen from Fig. 7 and Table II, is almost zero, reflecting an isotropic electron angular distribution, as is the case for the Ba I $[6p_{3/2}ns_{1/2}]_{J=1}$ series. The β(Ba II $6s_{1/2}$) value of ~ 1.3 for the Ba I $[6p_{1/2}ns_{1/2}]_{J=1}$ series is somewhat lower than the average value of 1.8 observed for the Ba I $[6p_{3/2}ns_{1/2}]_{J=1}$ states.

While most of our branching-ratio measurements do not involve resolution of the Ba II $5d$ fine-structure states of the ion, we have made a limited number of measurements which do resolve the Ba II $5d_{5/2}$ and $5d_{3/2}$ states.

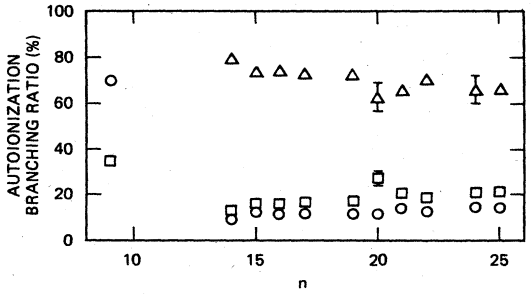

FIG. 8. Branching ratios for the Ba $[6p_{3/2}ns_{1/2}]_{J=1}$ states autoionizing to the Ba II $6s_{1/2}$ state (open circles), Ba II $5d$ state (open squares), and Ba II $6p_{1/2}$ state (for $n \geq 12$) (open triangles) plotted as a function of n. The autoionization branching ratios to the two possible Ba II $5d$ fine-structure states of the ion are unresolved in these measurements.

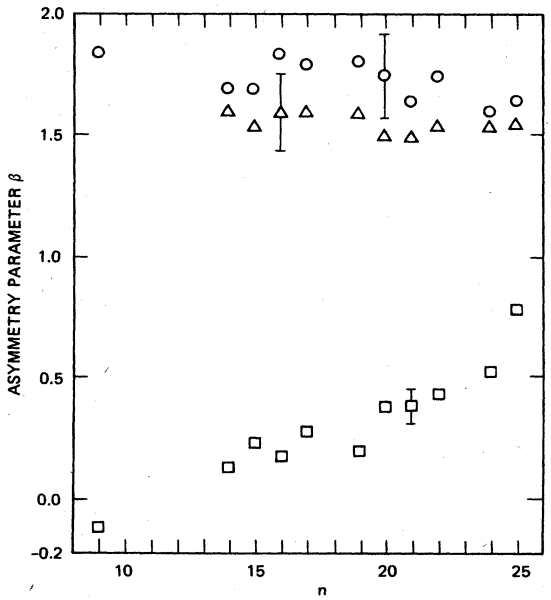

FIG. 9. Ejected-electron asymmetry parameter for the Ba $[6p_{3/2}ns_{1/2}]_{J=1}$ state autoionizing to the Ba II $6s_{1/2}$ state β(Ba II $6s_{1/2}$) (open circles); to the Ba II $5d$ state, β(Ba II $5d$) (open squares); and to the Ba II $6p_{1/2}$ state, β(Ba II $6p_{1/2}$) (open triangles) plotted as a function of n.

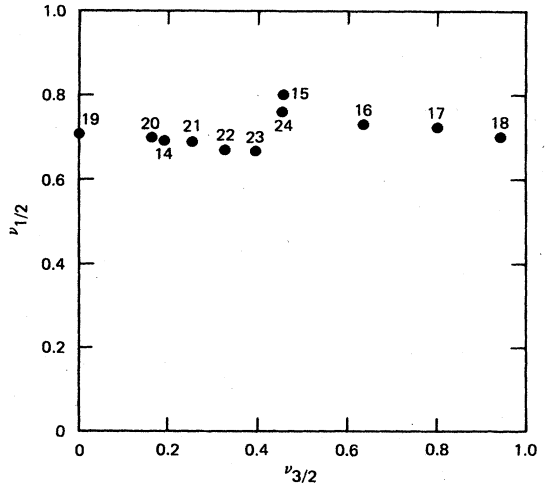

FIG. 10. Lu-Fano-type plot of the effective quantum number $\nu_{1/2}$ (modulo 1) relative to the Ba II $6p_{1/2}$ limit of the Ba $[6p_{1/2}ns_{1/2}]_{J=1}$ levels vs their effective quantum number $\nu_{3/2}$ (modulo 1) relative to the Ba II $6p_{3/2}$ limit. The numbers in the plot indicate the n value of the Ba $[6p_{1/2}ns_{1/2}]_{J=1}$ level. These values were obtained from Ref. 15.

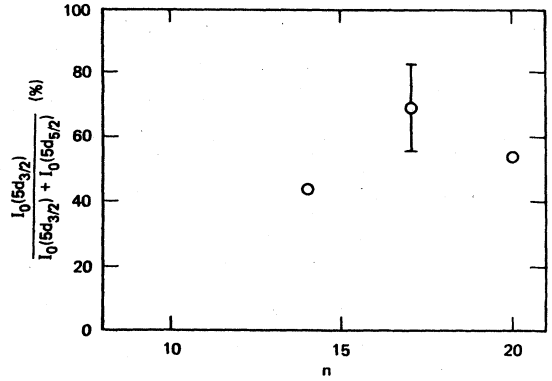

FIG. 11. The relative branching ratios for the autoionization of Ba $[6p_{1/2}ns]_{J=1}$ levels to the two $5d$ fine-structure states of Ba II. The relative branching ratio I_0(Ba II $5d_{3/2}$)/[I_0(Ba II $5d_{5/2}$)+I_0(Ba II $5d_{5/2}$)] (%) is plotted as a function of n (open circles). The errors shown represent the statistical uncertainty in our data.

Since the Ba II $5d$ fine structure is split by 801 cm^{-1}, the energy of the ejected electron differs by $\sim$0.1 eV for the two possible Ba II $5d_{5/2}$ and $5d_{3/2}$ final ion states. Given the 5% energy resolution of our analyzer, we must reduce the transmission energy to 1 eV, so that ΔE=0.05 eV. Using the energy analyzer in this high-resolution mode it is easy to resolve this 0.1-eV difference in the energies of the electron, albeit at a reduced value of the electron signal. The relative branching ratio for the autoionization of Ba I $[6p_{1/2}ns_{1/2}]_{J=1}$ levels to the Ba II $5d_{5/2}$ and $5d_{3/2}$ fine-structure ion states is plotted as a function of n in Fig. 11 and tabulated in Table V. Similar measurements for the Ba I $[6p_{3/2}ns_{1/2}]_{J=1}$ states are tabulated in Table VI and plotted in Fig. 12. The statistical uncertainty in these fine-structure-resolved measurements of β(Ba II $5d$) is large because the peak electron signal never exceeds 2—3 electrons per laser shot. Given the large statistical uncertainty in our data, we see little variation in the relative fine-structure rates, for both the Ba I $[6p_{3/2}ns_{1/2}]_{J=1}$ and Ba I $[6p_{1/2}ns_{1/2}]_{J=1}$ states. It is interesting to note that while the branching ratio I_0(Ba II $5d_{3/2}$)/[I_0(Ba II $5d_{3/2}$)+I_0(Ba II $5d_{5/2}$)] is approximately $\frac{1}{3}$ for the Ba I $[6p_{3/2}ns_{1/2}]_{J=1}$ states (see Fig. 12), it is considerably higher for the Ba I $[6p_{1/2}ns_{1/2}]_{J=1}$ states. This can be seen from Fig. 11, which shows I_0(Ba II $5d_{3/2}$)/I_0(Ba II $5d_{3/2}$)+I_0(Ba II $5d_{5/2}$)] ranging from 44% to 69% for the Ba I $[6p_{1/2}ns_{1/2}]_{J=1}$ states.

IV. THEORY

A. General angular properties

The photoexcitation process in general may lead either to the excitation of a structureless continuum or a structured continuum consisting of autoionizing states. The theory of the angular distribution of an electron ejected as a result of photoexcitation of an unpolarized target has been developed by Fano and Dill[27] using the concept of angular momentum transfer. The essence of this approach is that the angular distribution of the collision product (in our case the electron) is expressed as a sum of incoherent contributions corresponding to different magnitudes of the angular momentum $\vec{J}_t$ transferred to an unpolarized target (see below). The main advantage of this formulation is that instead of performing a coherent sum of the partial cross sections over J, the total angular momentum of the system, only a single incoherent sum over $\vec{J}_t$ is required.[27–29] However, in the present experiment there is only one value of the total angular momentum J, which is equal to one. The advantage of expressing the cross sections in terms of sums over $\vec{J}_t$ is lost. We therefore use the expansions in terms of the total angular momentum J of the system and use the notation of Fano and Dill.[27]

TABLE V. Relative branching ratios and β parameter for the autoionization of Ba $[6p_{1/2}ns_{1/2}]_{J=1}$ levels to the $5d_{3/2}$ and $5d_{3/2}$ fine-structure states of Ba II.

Ba I autoionizing state	Relative branching ratios to ion fine-structure state (%)		Electron asymmetry parameter	
	Ba II $5d_{3/2}$	Ba II $5d_{5/2}$	β(Ba II $5d_{3/2}$)	β(Ba II $5d_{5/2}$)
$6p_{1/2}14s_{1/2}$	44(10)	56	0.1(3)	0.65(40)
$6p_{1/2}17s_{1/2}$	69(10)	31	0.1(3)	−0.4(4)
$6p_{1/2}20s_{1/2}$	54(10)	46	0.1(4)	0.6(4)

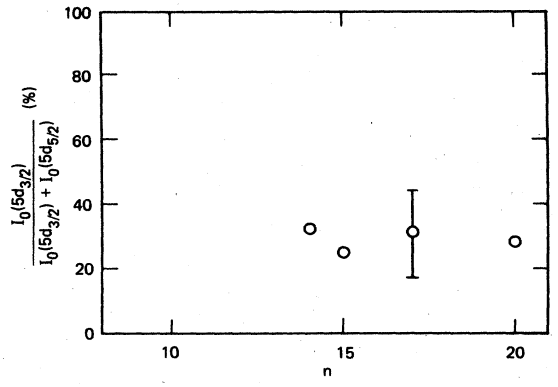

FIG. 12. The relative branching ratios for the autoionization of Ba $[6p_{3/2}ns]_{J=1}$ levels to the two $5d$ fine-structure states of Ba II. The relative branching ratio $I_0(\text{Ba II } 5d_{3/2})/[I_0(\text{Ba II } 5d_{5/2}) + I_0(\text{Ba II } 5d_{3/2})]$ (%) is plotted as a function of n (open circles).

Consider the process in which a photon with a well-defined polarization excites an atom from an unpolarized state to an autoionizing state, which subsequently autoionizes into an ion and electron. We can schematically write this as

$$X(J_0,\Pi_0)+\gamma(J_\gamma=1,\Pi_\gamma=-1) \rightarrow X^+(J_c,\Pi_c)+e^-(l,\Pi_e=(-1)^l)\ , \quad (3)$$

where X is the initial unpolarized atom and γ the incident photon. X^+ and e^- are the resulting ion and electron, respectively, resulting from the autoionization of the intermediate state. Here J_0 and J_γ refer to the angular momentum of the target atom and photon, respectively, while l is the orbital angular momentum of the ejected electron. The spins of the electron are coupled to the angular momentum of the ion J_c to give a resultant total angular momentum J_{cs}. The parity of each term in Eq. (3) is represented by Π and an appropriate subscript. Since the total angular momentum and the parity are conserved in the autoionization process, this requires

$$\vec{J}=\vec{J}_0+\vec{J}_\gamma=\vec{J}_{cs}+\vec{l} \quad (4a)$$

and

$$\Pi=\Pi_0\Pi_\gamma=\Pi_c(-1)^l\ . \quad (4b)$$

The angular momentum transferred in this reaction is given by[27,28]

$$\vec{J}_t=J_{cs}-\vec{J}_0=\vec{J}_\gamma-\vec{l}\ . \quad (4c)$$

The amplitude for the photoexcitation process indicated in Eq. (3) may be computed by first evaluating the matrix element

$$(J_{cs}m_{cs},lm\ |S\ |J_0m_0,J_\gamma m_\gamma)\ , \quad (5)$$

where S is the scattering matrix element.[27] In our experiments we start from an unaligned state with all possible values of m_0. In evaluating the total transition amplitude we have to average over the quantum number m_0. The theory is constructed for an unaligned initial state with all possible values of m_0. In our case we have $J_0=m_0=0$, which simplifies the averaging because only one state is involved. This is, of course, the simplest example of a more general case. Similarly, the orientation of the ion and the electron are unobserved; therefore, in evaluating the total transition amplitude the sum over m_{cs} is required.

The transition amplitude for the ejection of an electron, in the direction (θ,ϕ), following autoionization is proportional to

$$A(\theta,\phi)=\sum_{l,m} Y_{lm}(\theta,\phi)(J_{cs}m_{cs},lm\ |S\ |J_0m_0,J_\gamma m_\gamma)\ . \quad (6)$$

$A(\theta,\phi)$ can be reexpressed in terms of the total angular momentum representation as

$$A(\theta,\phi)=\sum_J\sum_l\sum_M Y_{lm}(\theta,\phi)(J_{cs}m_{cs},lm\ |JM)(JM\ |J_0m_0,J_\gamma m_\gamma)(J_{cs}l||S(J)||J_0J_\gamma)\ , \quad (7)$$

where $(J_{cs}l||S(J)||J_0J_\gamma)$ is a submatrix which is independent of M. If several J values result from the excitation of the initial state, then the above equation may be further simplified in terms of the angular momentum transfer representation of Dill and Fano.[27,28] However, if only one J value results in Eq. (7), as is the case in our experiment, then the angular momentum transfer representation provides no further simplification. We therefore drop the sum over J and M and rewrite $A(\theta,\phi)$ as

$$A(\theta,\phi)=\sum_l Y_{lm}(\theta,\phi)(J_{cs}m_{cs},lm\ |JM)(JM\ |J_0m_0,J_\gamma m_\gamma) \times(J_{cs}l||S(J)||J_0J_\gamma)\ , \quad (8)$$

TABLE VI. Relative branching ratios and β parameter for the autoionization of Ba $[6p_{3/2}ns_{1/2}]_{J=1}$ levels to the $5d_{1/2}$ and $5d_{3/2}$ fine-structure states of Ba II.

	Relative branching ratios to ion fine-structure state (%)		Electron asymmetry parameter	
Ba I autoionizing state	Ba II $5d_{3/2}$	Ba II $5d_{5/2}$	β(Ba II $5d_{3/2}$)	β(Ba II $5d_{5/2}$)
$6p_{3/2}14s_{1/2}$	32(10)	68	0.1(4)	0.0(3)
$6p_{3/2}15s_{1/2}$	25(10)	75	0.0(3)	0.0(3)
$6p_{3/2}17s_{1/2}$	31(10)	69	−0.1(4)	0.0(3)
$6p_{3/2}20s_{1/2}$	28(10)	72	0.0(3)	0.1(3)

where

$$m = m_0 + m_\gamma - m_{cs} \tag{9a}$$

and

$$M = m_0 + m_\gamma \, . \tag{9b}$$

The differential scattering cross section for the ejection of the electron along (θ,ϕ), $d\sigma(\theta,\phi)/d\Omega$ is proportional to the square of $A(\theta,\phi)$, summed over m_{cs} and averaged over m_0. This can be written as

$$B(\theta,\phi) = \frac{1}{2J_0+1} \sum_{m_0,m_{cs}} |A(\theta,\phi)|^2 \, . \tag{10}$$

$B(\theta,\phi)$ may be explicitly written as

$$B(\theta,\phi) = \sum_{l} \sum_{l'} \sum_{m_{cs}} \sum_{m_0} Y_{lm}(\theta,\phi) Y^*_{l'm}(\theta,\phi) (J_{cs} l || S(J) || J_0 J_\gamma)(J_{cs} m_{cs}, lm \mid JM) \mid (JM \mid J_0 m_0, J_\gamma m_\gamma) \mid^2$$
$$\times (J_0 J_\gamma || S^\dagger(J) || J_{cs} l')(JM \mid J_{cs} m_{cs}, l'm) \, . \tag{11}$$

Using the summation properties of the Clebsch-Gordan coefficients and the expansion

$$Y_{lm}(\theta,\phi) Y^*_{l'm}(\theta,\phi) = (-1)^m \frac{(2l+1)^{1/2}(2l'+1)^{1/2}}{4\pi} \sum_k (l0,l'0 \mid k0) P_k(\cos\theta)(k0 \mid lm, l'-m) \, , \tag{12}$$

where $P_k(\cos\theta)$ is the Legendre polynomial of order k, we get

$$B(\theta,\phi) = (-1)^{J_{cs}} \frac{(2l+1)^{1/2}(2l'+1)^{1/2}}{4\pi} \sum_{l,l',k} (J_{cs} l || S(J) || J_0 J_\gamma)(J_0 J_\gamma || S^\dagger(J) || J_{cs} l')$$
$$\times P_k(\cos\theta) \begin{pmatrix} J & J & k \\ M & -M & 0 \end{pmatrix} \begin{Bmatrix} J & J & k \\ l & l' & J_{cs} \end{Bmatrix} (l0,l'0 \mid k0) \, , \tag{13}$$

where the large curly brackets and the large parentheses refer to the 6-J and the 3-J symbols, respectively. Finally, since the spin orientation of the ion and the electron are unobserved we sum the expression for $B(\theta,\phi)$ [Eq. (13)] over the various values of J_{cs} to obtain an expression for the angular distribution. We note that the symmetry of the 3-J symbol and the dipole excitation from the initial state only allow $k=0$ or 2 in Eq. (13). The differential cross section for the ejection of electrons can therefore be expressed as

$$\frac{d\sigma}{d\Omega} = \frac{\sigma}{4\pi}[1+\beta P_2(\cos\theta)] \, , \tag{1'}$$

where σ is the total cross section. This expression for the angular distribution is exactly the form predicted by Yang's theorem,[23] referred to earlier.

It is also clear from Eqs. (13) and (1') that B contains most of the information pertaining to the matrix elements of S which are the only unknowns in this problem. It is interesting to note that, even though the observed β parameter is an average over the unobserved values of J_{cs}, the ratio of the matrix element of S in Eq. (13) can be determined.

To illustrate the power of the general results of Eq. (13) we consider some specific examples. First consider the Ba autoionization process

$$\mathrm{Ba}([6s_{1/2}ns_{1/2}]_{J=0}) + \gamma \rightarrow \mathrm{Ba\ II}(6s_{1/2}) + e^-(\epsilon l \ (l=1)) \, . \tag{14}$$

To obtain the angular distribution for the electrons, the expression in Eq. (13) must be summed over J_{cs}. For the autoionization channel represented in Eq. (14), J_{cs} is either 0 or 1, which corresponds to the parity-favored and parity-unfavored transitions, respectively.[28] Using the notation

$$S^{(J_{cs})} = (J_{cs}, l || S(J=1) || J_0=0, J_\gamma=1) \, , \tag{15}$$

we obtain from Eq. (13)

$$\frac{d\sigma}{d\Omega} = C(|S^{(0)}|^2 + |S^{(1)}|^2) \times \left[1 + P_2(\cos\theta) \frac{2|S^{(0)}|^2 - |S^{(1)}|^2}{|S^{(0)}|^2 + |S^{(1)}|^2}\right] , \tag{16}$$

where C is a constant independent of J_{cs}. From the form of the above expression we can express $\beta(\mathrm{Ba\ II}\ 6s_{1/2})$ and $\sigma(\mathrm{Ba\ II}\ 6s_{1/2})$ as

$$\beta(\mathrm{Ba\ II}\ 6s_{1/2}) = \frac{2|S^{(0)}|^2 - |S^{(1)}|^2}{|S^{(0)}|^2 + |S^{(1)}|^2} \tag{17}$$

and

$$\sigma(\mathrm{Ba\ II}\ 6s_{1/2}) = C(|S^{(0)}|^2 + |S^{(1)}|^2) \, , \tag{18}$$

where $\sigma(\mathrm{Ba\ II}\ 6s)$ is the cross section for the autoionization process indicated in Eq. (14). It is also clear from Eq. (16) that $\beta=2$ if $S^{(1)}=0$, as would be the case in the Cooper-Zare model.[30] However, as our experimental results indicate, $\beta(\mathrm{Ba\ II}\ 6s_{1/2}) \simeq 1.8$ for the Ba I $[6p_{3/2}ns_{1/2}]_{J=1}$ states, which means that $|S^{(0)}|^2/|S^{(1)}|^2 = 14$, while $\beta(\mathrm{Ba\ II}\ 6s_{1/2}) \simeq 1.4$ for the Ba I $[6p_{1/2}ns_{1/2}]$ states leads to $|S^{(0)}|^2/|S^{(1)}|^2 = 4$. The relative importance of the matrix element $S^{(1)}$, which leads to the parity-unfavored transition,[31] is very different depending on whether the Ba I $[6p_{1/2}ns_{1/2}]_{J=1}$ or Ba I $[6p_{3/2}ns_{1/2}]_{J=1}$ states are excited.

Let us digress for a moment on the physical signifi-

cance of the matrix elements $S^{(1)}$ and $S^{(0)}$ for the process represented by Eq. (14) and their relative importance. In the present work the photoexcitation to the Ba I $[6p_{1/2\,(3/2)}ns_{1/2})]_{J=1}$ autoionizing state starts from the Ba I $6sns\ ^1S_0$ bound state. Before the photoabsorption, the spin of the Rydberg electron and the core electron are aligned antiparallel as in a singlet state. In the absence of any spin-orbit, or orbit-orbit, Coulomb exchange interaction in the final autoionizing state, the spin of the ejected and the core electrons would remain antiparallel or singlet, yielding $J_{cs}=0$. On the other hand, if the ejected-electron spin is parallel to that of the core, then $J_{cs}=1$. The size of $S^{(1)}$ relative to $S^{(0)}$ or, in other words, the departure of β from 2 reflects directly the importance of the anisotropic Rydberg-electron—core interactions at small radii (spin-orbit and exchange interactions). In terms of the angular momentum transfer formulation, the angular momentum transferred $\vec{J}_t$ is given by $\vec{J}_t=\vec{J}_{cs}-\vec{J}_0$. In our case $\vec{J}_0=\vec{0}$, therefore $\vec{J}_t=\vec{J}_{cs}$. The two resulting values of $J_t=0$ and 1 correspond to the parity-favored and parity-unfavored transitions, respectively.[28]

An initially surprising result is observed in the excitation of the Ba I $[6p_{3/2}ns_{1/2}]_{J=1}$ state with $n\geq 12$ and its subsequent autoionization to the Ba II $6p_{1/2}$ state of the ion, which can be written as

$$\mathrm{Ba}([6p_{3/2}ns_{1/2}]_{J=1})+\gamma \rightarrow \mathrm{Ba\ II}(6p_{1/2})+e^-(\epsilon l\ (l=0,2))\ . \quad (19)$$

In this case we only have parity-favored transitions with $J_{cs}=0$ or 2, when $l=0$ or 2, respectively. Using Eq. (13) we obtain for β(Ba II $6p_{1/2}$)

$$\beta(\mathrm{Ba\ II}\ 6p_{1/2})=|S^{(2)}|^2-2^{1/2}[(S^{(0)}+S^{(2)})+\mathrm{c.c.}]/(|S^{(0)}|^2+|S^{(2)}|^2) \quad (20)$$

and

$$\sigma(\mathrm{Ba\ II}\ 6p_{1/2})\propto |S^{(0)}|^2+|S^{(2)}|^2\ , \quad (21)$$

where c.c. indicates complex conjugate and σ(Ba II $6p_{1/2}$) is the cross section for the autoionization process indicated in Eq. (19). If we assume that only $l=2$ electrons are ejected, then $\beta=1$. On the other hand, if only the s electrons ($l=0$) are ejected, then $\beta=0$, as would be expected. Since both the $l=0$ and $l=2$ electrons are ejected in general, one would at first glance expect the asymmetry parameter to lie between 0 and 1. However, this is not the case, as can be seen from Table IV. The measured value of β(Ba II $6p_{1/2}$) is about 1.5. From Eq. (20) it is clear that $\beta>1$ when $S^{(0)}$ and $S^{(2)}$ are of opposite sign. Thus it is quite evident from this example that a very simple picture of predicting the asymmetry parameter by incoherent addition does not work because of the interference between electrons of different orbital angular momenta.

From the discussion of general angular properties of the specific reaction considered above, it is clear that many physical insights are obtained without the knowledge of any specific matrix element. Specifically, this analysis shows, for instance, the relative importance of the anisotropic Rydberg-electron—core interactions for the various autoionization channels.

B. Evaluation of radial matrix elements by MQDT

While the angular terms in Eq. (13) are easily calculable, the matrix elements in the summation require a knowledge of the radial electron wave function. Clearly, *ab initio* calculations of these reduced matrix elements are difficult, although it is possible in principle to reduce these matrix elements in terms of the MQDT parameters. Since in the present experiment $J_0=0$, we use this particular value of J_0 to evaluate the matrix element of S in terms of the dipole moment operator:[27]

$$((J_c s)J_{cs},lJ||S(J)||J_0,J_\gamma=1) = n(2J+1)^{-1/2}((J_c s)J_{cs}l,J-||D||J_0=0)\ , \quad (22)$$

where J_c is the angular momentum of the core, D is the dipole moment operator, and n is a constant of proportionality. The minus sign in the matrix element refers to the normalization of the wave function with the incoming-wave boundary condition. We note that the above expression is true only for $J_0=0$, although similar expressions may be obtained for nonzero values of J_0. Although our expressions for the matrix elements of S hereon are evaluated for a particular value of J_0, we continue to use J_0 in the following expressions with the understanding that $J_0=0$.

It is instructive to consider the excitation and decay of the Ba I $[6p_{1/2\,(3/2)}ns_{1/2}]_{J=1}$ states in the following picture. First the Ba I $[6s_{1/2}ns_{1/2}]_{J=0}$ initial bound Rydberg state absorbs a photon and is excited to the Ba I $[6p_{1/2\,(3/2)}ns_{1/2}]_{J=1}$ autoionizing state. During the excitation process the initial Rydberg electron spends most of its time far away from the core region, and the electronic wave function is best characterized by the dissociative-channel wave functions $|j\rangle$ (Ref. 7) which are assumed to be jj coupled and the transition amplitude by the dipole transition matrix elements

$$D_{ij}=\langle i\,|\,D\,|\,j\rangle \quad (23)$$

connecting the initial dissociative channel state $|j\rangle$ with the final dissociative state $|i\rangle$.[14] While the dissociative channels can in general be either open or closed, in the present experiment both $|i\rangle$ and $|j\rangle$ are closed. The eigenfunctions of the autoionizing state are not the dissociative channel states, but the collision eigenstate $|\rho\rangle$ (the number of collision eigenstates $|\rho\rangle$ equals the number of open channels). The dissociative-channel states $|i\rangle$ are

related to the collision eigenstates $|\rho\rangle$ by[9,10]

$$|\rho\rangle=\sum_i T_{i\rho}|i\rangle\ , \tag{24}$$

where $T_{i\rho}$ is the transformation matrix element connecting the dissociative and collision eigenstates. The reduced matrix element may therefore be expressed as

$$((J_c s)J_{cs},lJ||D||J_0) = \sum_{\rho,i}((J_c s)J_{cs},lJ\,|\,i=J_c(ls)jJ)D_{i_b}T_{i\rho}T_{i_b\rho}\ , \tag{25}$$

where j and s refer to the total angular momentum and spin of the Rydberg electron, respectively, while J refers to the angular momentum of the whole system (ion + electron). In Eq. (25) we have assumed that the initial bound Rydberg state is described by a single closed dissociative state which is connected to the autoionizing state by a single closed dissociative state $|i_b\rangle$. Therefore,

$$D_{i_b}=\langle i_b\,|\,D\,|\,J_0\rangle\ , \tag{26}$$

where $|J_0\rangle$ is the initial Rydberg state Ba I $[6s_{1/2}ns_{1/2}]_{J=0}$.

The transformation or the angular momentum recoupling in the sum in Eq. (25) is required since the dissociative-channel wave function assumes the jj coupling whereby the spin of the ejected electron is coupled to its own orbital angular momentum $j=\vec{l}+\vec{s}$. However, in setting up our initial problem we have chosen to couple the unobserved spin of the electron with the unobserved orientation of the ion. Using the angular momentum recoupling identities we obtain

$$((J_c s)J_{cs},lJ\,|\,D\,|\,J_0)=(-1)^{J_c+3/2+l}(2J_{cs}+1)^{1/2}\sum_l\sum_{j=l\pm1/2}(2j+1)^{1/2}\begin{Bmatrix}\frac{1}{2} & l & j\\ 1 & J_c & J_{cs}\end{Bmatrix}T_{i\rho}T_{i_b\rho}D_{i_b}\ . \tag{27}$$

Since the i channel (dissociative) wave functions use the standing-wave normalization, we multiply these wave functions by the Coulomb phase factor to obtain the wave function with incoming-wave normalization. The phase factor is given by

$$i^{-l}\exp[i(\Delta_{lJ_c}+\pi\tau_\rho)]\ ,$$

where Δ_{lJ_c} is the Coulomb phase given by $\arg\Gamma(l+1-i/k)$ which is determined by l and the kinetic energy $k^2/2$ (in atomic units), and τ_ρ is the eigenphase shift of the collision eigenstate $|\rho\rangle$. Combining Eqs. (25) and (27), we obtain for the reduced matrix element

$$((J_c s)J_{cs},lJ\,|\,D\,|\,J_0)=n(2J+1)^{-1/2}i^{-l}e^{i\Delta_{lJ_c}}(-1)^{J_c+3/2+l}(2J_{cs}+1)^{1/2}D_{i_b}\sum_{\rho,i}(2j+1)^{1/2}\begin{Bmatrix}\frac{1}{2} & l & j\\ 1 & J_c & J_{cs}\end{Bmatrix}T_{i\rho}T_{i_b\rho}e^{i\pi\tau_\rho}\ . \tag{28}$$

Combining the above equation with Eq. (13) we can calculate $d\sigma/d\Omega$. The ejected-electron angular distribution $d\sigma/d\Omega$ can now be obtained by combining Eqs. (13) and (28).

C. A simplified analysis of the Ba I $[6p_{1/2}ns_{1/2}]_{J=1}$ autoionizing states

In analyzing the autoionization of the Ba I $[6p_{1/2}ns_{1/2}]_{J=1}$ states, it is clear that a complete analysis of the problem in terms of the MQDT parameters is difficult. This difficulty stems from the large number of open channels associated with the autoionizing state considered here. In order to simplify the analysis only a small number of channels can be used. Specifically, we choose three open channels and one closed channel, which characterizes the bound part of the autoionizing Ba I $[6p_{1/2}ns_{1/2}]_{J=1}$ state. The four channels with three ionization limits are

	1	2	3	4
$\|\alpha\rangle$	$^1P_1$	$^3P_1$	$^3X_1$	$^{1,3}P_1$
$\|i\rangle$	$6s_{1/2}\epsilon p_{3/2}$	$6s_{1/2}\epsilon p_{1/2}$	$5d_j\epsilon p_{3/2}$	$6p_{1/2}ns_{1/2}$

where $|\alpha\rangle$ and $|i\rangle$ refer to the close-coupled-channel and the dissociative-channel wave function,[7,9] respectively. The symbol X in the entry for the close-coupled channel represents the fact that no unique assignment for these channels is possible given the limited number of channels. Since the basis set listed above uses all the open channels required for the autoionization process,

$$\mathrm{Ba}([6p_{1/2}ns_{1/2}]_{J=1})\rightarrow\mathrm{Ba\ II}(6s_{1/2})+e^-(\epsilon p_{1/2\,(3/2)})\ , \tag{29}$$

we can calculate β(Ba II $6s_{1/2}$) even in this four-channel approximation. The six open channels associated with the $5d_{3/2\,(5/2)}\epsilon p,\epsilon f$ continuum are approximated with one open channel. This is, of course, a crude approximation, but it allows us to compute to the lowest approximation the branching ratios for the autoionization to the Ba II $6s$ and $5d$ state of the ion. If the elements of $U_{i\alpha}$ along with the four eigendefects μ_α are treated as free parameters, then the fit to the experiment has ten independent parameters.

The basic parameters of the MQDT analysis are the set of eigendefects μ_α, as well as the matrix $\underline{U}$ which relates

the close-coupled wave functions $|\alpha\rangle$ to the dissociative wave functions $|i\rangle$.[7,9] If we assume interaction between all four channels, then we have six independent elements $U_{i\alpha}$ of $\underline{U}$. These, along with eigendefect μ_α, lead to a total of ten independent parameters. Clearly, any MQDT fit with ten independent parameters in the present context is meaningless. We must therefore make reasonable assumptions to reduce the number of free parameters. To start with, we assume that a pure *jj-LS* coupling occurs between the first two channels. The interaction between the Ba I bound $6p_{1/2}ns_{1/2}$ channel and the three open channels is introduced by defining three independent interaction angles θ_{14}, θ_{24}, and θ_{34}, where θ_{ij} is the interaction angle between channels i and j. Note that all other mixing angles are set equal to zero. The matrix $\underline{U}$ is a product of rotation matrices $\underline{R}(\theta_{ij})$ defined in Ref. 10. Explicitly in our case,

$$\underline{U}=\underline{R}(\theta_{14})\underline{R}(\theta_{24})\underline{R}(\theta_{34}) . \tag{30}$$

Note that θ_{34} is zero if there is no configuration mixing between the Ba I $6p_{1/2}ns_{1/2}$ and $5d_j\epsilon p_{j'}$ series. The number of parameters can be further reduced by fixing the values of μ_1, μ_2, and μ_3. We use the values $\mu_1=0.79$ and $\mu_2=0.81$ obtained by Armstrong *et al.*[5] by fitting the bound $J=1$ odd-parity states in Ba. If we further assume that the autoionization to the Ba II $5d$ state proceeds predominantly with the ejection of ϵp electrons, then we can use the value of $\mu_3=0.5$ for the Ba I $5dn'p\ ^1P_1$ closed coupled channel from Ref. 5. This is somewhat arbitrary, since other Ba I closed coupled channels, $5dnp\ ^3P_1$ and $5dnp\ ^3D_1$, are also involved.

The problem of fitting the Ba I $[6p_{1/2}ns_{1/2}]_{J=1}$ autoionization data to MQDT now involves only four free parameters—the three mixing angles θ_{14}, θ_{24}, and θ_{34} and the eigendefect μ_4. Although the position and width of the autoionizing Ba I $[6p_{1/2}ns_{1/2}]_{J=1}$ levels are known, no MQDT fit on this series has been reported. It is clear that by using μ_4 as a free parameter we can calculate the quantum defect for the Ba I $6p_{1/2}ns_{1/2}$ series and fit to its experimental value of 0.72 (modulo 1). With the remaining three parameters (the mixing angles) we fit the width of the autoionizing line, the electron asymmetry parameter β(Ba II $6s_{1/2}$), and the branching ratio to the Ba II $6s$ and $5d$ state of the ion, respectively. As the branching ratios and the asymmetry parameter β(Ba II $6s_{1/2}$) show variations in n, we use the values of branching ratios and β which lie near the flat part of the plot in Figs. 6 and 7, respectively. In this four-channel MQDT fit we use the experimental value of 0.18 for the branching ratio to the Ba II $6s_{1/2}$ state of the ion and β(Ba II $6s_{1/2}$)=1.4. The width of Ba I $[6p_{1/2}ns_{1/2}]_{J=1}$ autoionizing states is approximately 0.10 (in units of n^{-3}) near $n=16$ and 17.[15]

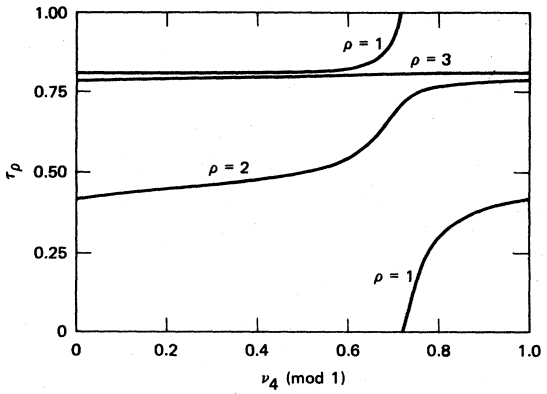

FIG. 13. Calculated τ_ρ (using the MQDT parameters listed in Table VII) plotted as a function of ν_4 (modulo 1). The three eigenphases $\pi\tau_\rho$ ($\rho=1-3$) and the corresponding collision eigenstates $|\rho\rangle$ constitute the eigenvalues and eigenfunctions in the autoionizing part of the spectrum.

Before we discuss the results obtained from this simplified model, we outline the details of the calculations based on MQDT. In the MQDT model under consideration, there are three open channels ($i=1$, 2, and 3) and one closed channel ($i=4$). The energy E of the Ba II bound $[6p_{1/2}ns_{1/2}]_{J=1}$ states is given by

$$E-I=-1/2\nu_4^2 , \tag{31}$$

where ν_4 is the effective quantum number of these states relative to the ionization limit I of the Ba II $6p_{1/2}$ state. The first step in this analysis is to obtain the eigenfunction of the Ba I autoionizing states. The eigenfunctions are the collision eigenstates $|\rho\rangle$ given by

TABLE VII. MQDT parameters used for the fit of the experimental data pertaining to the autoionization of Ba I $[6p_{1/2}ns_{1/2}]_{J=1}$ levels near $n=16$ and 17 (see Sec. IV C). The width of the levels is in units of n^3, while the position is indicated in terms of effective quantum number (modulo 1).

i,α	1	2	3	4
μ_α	0.79	0.81	0.5	0.23
$U_{i\alpha}$	0.81	0.57	−0.08	0.14
	−0.57	0.82	0.01	−0.03
	0.0	0.0	0.88	0.48
	−0.15	−0.07	−0.47	0.87
	$\theta_{14}=0.15$	$\theta_{24}=0.07$	$\theta_{34}=0.5$	
	Position	Width	β(Ba II $6s_{1/2}$)	I_0(Ba II $6s$)/[I_0(Ba II $6s$)+I_0(Ba II $5d$)]
Experiment	0.72	0.10	1.46	18%
Theory	0.72	0.10	1.46	19%

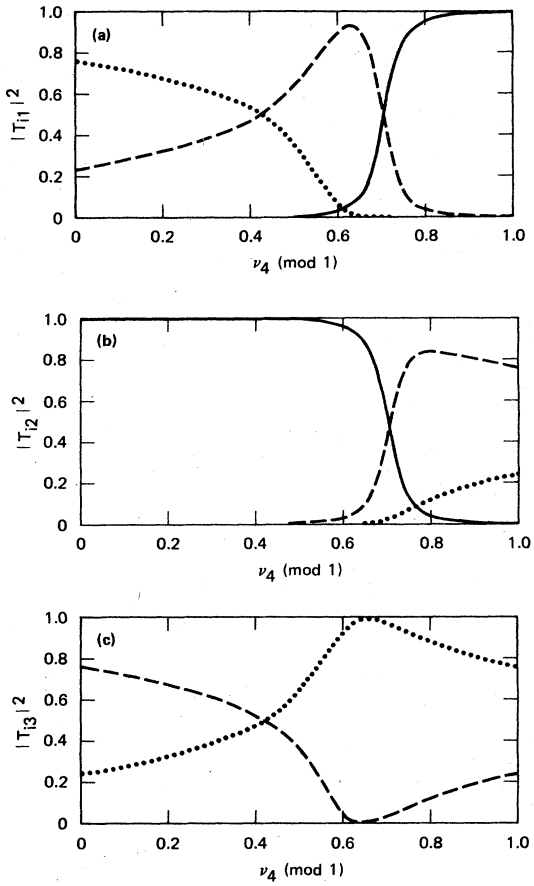

FIG. 14. Transformation matrix elements $|T_{i\rho}|^2$ plotted as a function of ν_4. When the index i takes the values 1–3, the matrix element $T_{i\rho}$ represents the amount of dissociative channel $|i\rangle$ mixed in a collision eigenstate $|\rho\rangle$. The index i in the plot is represented as (— — —) ($i=1$), (. . .) ($i=2$), (——) ($i=3$). (a), (b), and (c) show $|T_{i\rho}|^2$ for $\rho=1$–3, respectively.

$$|\rho\rangle = T_{4\rho}|i=4\rangle + \sum_{\substack{\text{open channels}\\(i=1,2,3)}} T_{i\rho}|i\rangle\ , \tag{32}$$

where $T_{i\rho}$ is the transformation matrix connecting the dissociative and the collision eigenstates.[9] The continuum normalization requires that $\sum_i |T_{i\rho}|^2=1$, where the sum is over the open channels ($i=1$, 2, and 3). Since the number of collision eigenstates $|\rho\rangle$ equals the number of open channels, the complete description of the eigenfunctions requires the knowledge of the transformation matrix elements $T_{i\rho}$ ($\rho=1$–3 and $i=1$–4). For a given choice of matrix elements $\mu_{i\alpha}$ [see Eq. (30)] and eigendefects μ_α we can solve for the eigenphase shifts $\tau_\rho(\nu_4)$ and transformation matrix element $T_{i\rho}$ for any value of ν_4. Since the procedure for computing τ_ρ and $T_{i\rho}$ is given elsewhere[9] we do not discuss it here. Once $T_{i\rho}$ and τ_ρ are known, the asymmetry parameter β(Ba II $6s_{1/2}$) and the branching ratio may be easily calculated using Eqs. (28) and (13).

The experimental values and the MQDT fit are shown in Table VII where the parameters θ_{14}, θ_{24}, θ_{34}, and μ_4 are listed. The agreement between the fit and the experiment

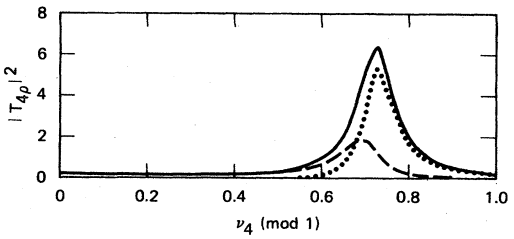

FIG. 15. Plot of $|T_{41}|^2$ (. . .), $|T_{42}|^2$ (— — —), and $\sum_\rho |T_{4\rho}|^2$ (——) as a function of ν_4. $|T_{43}|^2$ is negligible on this scale.

is quite good. Using the MQDT parameters listed in Table VII we have plotted the functional forms of some matrix elements and phase shifts to illustrate the fitting procedure outlined above. The Fig. 13 eigenphase shifts $\tau_\rho(\nu_4)$ ($\rho=1$–3) are plotted as a function of ν_4. This type of plot is conventionally known as the Lu-Fano plot. The matrix elements $|T_{i\rho}|^2$ for the open channels ($i=1$–3) are plotted as a function of ν_4 for each collision eigenstate ρ, in Fig. 14. Similarly, the functional form of the matrix elements $|T_{4\rho}(\nu_4)|^2$ are plotted in Fig. 15. Note that the autoionization line shape of the bound states, which are the Ba I $[6p_{1/2}ns_{1/2}]_{J=1}$ states in this example, is given by $\sum_\rho |T_{4\rho}(\nu_4)|^2$. Interestingly, from Fig. 15 we see that there is almost no contribution to the line shape from the $\rho=3$ collision eigenchannel. We also note that the calculations indicate no change in β(Ba II $6s_{1/2}$) as a function of energy, as would be expected if the continuum excitation is neglected.

D. A simplified analysis of the autoionization of Ba I $[6p_{3/2}ns_{1/2}]_{J=1}$ states to the Ba II $6p_{1/2}$ state of the ion

Using the four-channel MQDT we have also attempted to fit the autoionization of the Ba I $[6p_{3/2}ns_{1/2}]_{J=1}$ ($n\geq 12$) to the Ba II $6p_{1/2}$ state of the ion. As in the previous example we choose three open channels and one closed channel, which characterizes the bound part of the Ba I $[6p_{3/2}ns_{1/2}]_{J=1}$ state. The four channels with three ionization limits are

	1	2	3	4
$\|\alpha\rangle$	$^1P_1$	$X_{J=1}$	$X_{J=1}$	$^{3,1}P_1$
$\|i\rangle$	$6p_{1/2}\epsilon s_{1/2}$	$6p_{1/2}\epsilon d_{3/2}$	$5d_{5/2}\epsilon p_{3/2}$	$6p_{3/2}ns_{1/2}$

The symbol X in the entry for the close coupled channels represents the fact that no unique assignment for these channels is possible given the limited number of channels. Since the autoionization to the Ba II $6p_{1/2}$ state of the ion involves only two open channels Ba I $6p_{1/2}\epsilon s_{1/2}$ and Ba I $6p_{1/2}\epsilon d_{3/2}$ which are included in the three open channels listed above, the autoionization parameters for this decay channel can be fit. For instance, β(Ba II $6p_{1/2}$) can be computed from Eq. (13) because all the open and closed channels are included. The third open channel Ba I $5d\epsilon p$ is chosen to approximate the remaining eight open chan-

TABLE VIII. MQDT parameters used for the fit of the experimental data pertaining to the autoionization of Ba I $[6p_{3/2}ns_{1/2}]$ states near $n=20$ (see Sec. IV D). The width of the states is in units of n^3, while the position is indicated in terms of effective quantum number (modulo 1).

i,α	1	2	3	4
μ_α	0.22	0.68	0.5	0.25
$U_{i\alpha}$	0.94	0.15	0.13	−0.28
	0.0	0.90	−0.19	0.39
	0.0	0.0	0.90	0.43
	0.34	−0.41	−0.37	0.76
	$\theta_{14}=-0.35$	$\theta_{24}=0.45$	$\theta_{34}=0.45$	

	Position	Width	β(Ba II $6p_{1/2}$)	Autoionization branching ratio to the Ba II $6p_{1/2}$ state
Experiment	0.7	0.2	1.5	72%
Theory	0.7	0.2	1.43	67%

nels converging either to the Ba II $6s$ or the Ba II $5d_{5/2\,(3/2)}$ limits of the Ba^+ core. This assumption is not too severe as the dominant autoionization decay of the Ba I $[6p_{3/2}ns_{1/2}]_{J=1}$ states is to the Ba II $6p_{1/2}$ state of Ba^+. We also note that the labeling of the third open channel is somewhat arbitrary. The interaction between the channels is introduced through the three mixing angles θ_{14}, θ_{24}, and θ_{34}. We neglect any explicit interaction between other channels and so all other mixing angles are set equal to zero. To reduce the number of free parameters in the fit, as in the previous example, we must make additional approximations. The values of μ_1 and μ_2 are fixed by using the values 0.22 and 0.68 obtained by Gounand *et al.*[14] in the fit of the Ba I $[6p_{1/2}nd]_{J=3}$ and Ba I $[6p_{3/2}nd]_{J=3}$ interacting autoionizing series.

While our implicit assumption that the μ's obtained by Gounand *et al.* for $J=3$ series are the same for $J=1$ series is tenuous, we nevertheless use these parameters to see if a reasonable fit can be obtained. Of course, if we were to use the true values for μ_1 and μ_2 (which are unknown at present) a different set of best-fit parameters pertaining to θ_{ij}'s would result. However, at this point we are merely interested in finding out if any fit to the experimental data can be obtained by using the minimal four-channel MQDT and some reasonable set of fixed initial parameters. Following the assumptions outlined above, the problem of fitting the Ba I $[6p_{3/2}ns_{1/2}]_{J=1}$ autoionization data to MQDT reduces to four free parameters—the three mixing angles θ_{14}, θ_{24}, and θ_{34}, and the eigendefect μ_4. The matrix $\underline{U}$ in terms of θ_{ij}'s is again given by Eq. (30). By using μ_4 as the free parameter we fit the position of the Ba I $[6p_{3/2}ns_{1/2}]_{J=1}$ states to the experimental value of 0.70 (modulo 1) for its quantum defect.[15] With the remaining three parameters (the mixing angles) we fit the width of the autoionizing line, the electron asymmetry parameter β(Ba II $6p_{1/2}$), and the branching ratio to the Ba II $6p_{1/2}$ state of the ion. We use the following experimental values for the fit: β(Ba II $6p_{1/2}$)$=1.5$ and the branching ratio to the Ba II $6p_{1/2}$ state of 72%. The experimental width of the Ba I $[6p_{3/2}ns_{1/2}]_{J=1}$ states near $N=15$ is 0.2 (in units of n^{-3}).[15]

The experimental values and the MQDT fit are shown in Table VIII, where the best-fit parameters θ_{14}, θ_{24}, θ_{34}, and μ_4 are also listed. The MQDT fit is quite reasonable and it illustrates that these complex data can in principle be fit to a few parameters. Unfortunately, many of the MQDT parameters, for example, μ's, are unknown at the present. As these parameters (μ's and θ_{ij}'s) become known, the β parameters and the branching ratio can be better fit to a more realistic MQDT formulation using more channels.

V. CONCLUSION

We have made comprehensive measurements of the branching ratios and the angular distributions of the electrons ejected from the autoionization of Ba $[6p_{1/2\,(3/2)}ns_{1/2}]_{J=1}$ states to the ground and excited states of Ba^+. The high resolution of the electron energy analyzer in conjunction with the detection of the ions has enabled us to measure the autoionizing branching ratios and electron angular distributions to the 0.090-MeV-split fine-structure states of Ba^+ $5d$ states. We do not find any variation in the ejected-electron β parameter or the autoionization branching ratio to the allowed ion states, as the excitation laser is swept across the autoionization linewidth of these states. This observation is a direct consequence of the stepwise excitation scheme used in this experiment.

From our measurements of the ejected-electron angular distributions and branching ratios the perturbation of the Ba I $[6p_{1/2}ns_{1/2}]_{J=1}$ series near $n=15$ and 23 is clearly evident. While the perturbations in this series also show up as variations in the position and widths of the levels of this series, the electron angular distributions are a much more sensitive probe of these perturbations and also provide the phase information. A rather surprising result emerging from our measurements is that the Ba I $[6p_{1/2\,(3/2)}ns_{1/2}]_{J=1}$ states predominantly autoionize to the excited states of the ion. This result has important

implications for the phenomena of dielectronic recombination and the development of autoionization lasers.

Several other important general features emerge from the analysis of the electron angular distribution data. From the measurement of β(Ba II $6s_{1/2}$) we conclude that the core-electron anisotropic interactions (spin-orbit and exchange interactions) are much more important for the Ba I $[6p_{1/2}ns_{1/2}]_{J=1}$ series than for the Ba I $[6p_{3/2}ns_{1/2}]_{J=1}$ series. The large electron asymmetry parameter associated with the autoionization of the Ba I $[6p_{3/2}ns_{1/2}]_{J=1}$ state to the Ba II $6p_{1/2}$ state of the ion indicates an interference between the $l=0$ and 2 outgoing electrons. Finally, we have recast MQDT to fit this situation and performed some preliminary fits to our data using the MQDT. The complete fitting requires some additional spectroscopic parameters that are not yet available.

ACKNOWLEDGMENTS

This work is supported by the U.S. Department of Energy (Office of Basic Energy Sciences) under Contract No. DE-AT03-79ER10376. We are pleased to acknowledge extremely useful discussions with D. L. Huestis.

---

*Permanent address: Laboratoire Aimé Cotton, C.N.R.S. II Batiment 505, 91405 Orsay Cedex, France.

[1]J. R. Rubbmark, S. A. Borgström, and K. Bockasten, J. Phys. B **10**, 421 (1977).
[2]M. Aymar and O. Robaux, J. Phys. B **12**, 531 (1979).
[3]J. J. Wynne and J. P. Hermann, Opt. Lett. **4**, 106 (1979).
[4]M. Aymar, P. Camus, M. Dieulin, and C. Morillon, Phys. Rev. A **18**, 2173 (1978).
[5]J. A. Armstrong, P. Esherick, and J. J. Wynne, Phys. Rev. A **15**, 180 (1977).
[6]P. Esherick, Phys. Rev. A **15**, 1920 (1977).
[7]U. Fano, Phys. Rev. A **2**, 353 (1970).
[8]U. Fano, J. Opt. Soc. Am. **65**, 797 (1975).
[9]K. T. Lu, Phys. Rev. A **4**, 579 (1971).
[10]C. M. Lee and K. T. Lu, Phys. Rev. A **8**, 241 (1973).
[11]W. E. Cooke, T. F. Gallagher, S. A. Edelstein, and R. M. Hill, Phys. Rev. Lett. **40**, 178 (1978).
[12]W. E. Cooke and T. F. Gallagher, Phys. Rev. Lett. **41**, 1648 (1978).
[13]W. E. Cooke and S. A. Bhatti, Phys. Rev. A **26**, 391 (1982).
[14]F. Gounand, T. F. Gallagher, W. Sandner, K. A. Safinya, and R. Kachru, Phys. Rev. A **27**, 1925 (1983).
[15]S. A. Bhatti and W. E. Cooke (unpublished).
[16]S. A. Bhatti, C. L. Cromer, and W. E. Cooke, Phys. Rev. A **24**, 161 (1981).
[17]J. Bokor, R. R. Freeman, and W. E. Cooke, Phys. Rev. Lett. **48**, 1242 (1982).
[18]W. R. S. Garton and K. Codling, Proc. Phys. Soc. London **75**, 87 (1960).
[19]C. M. Brown and M. L. Ginter, J. Opt. Soc. Am. **68**, 817 (1978).
[20]U. Fano, Phys. Rev. **124**, 1866 (1961).
[21]N. H. Tran, R. Kachru, and T. F. Gallagher, Phys. Rev. A **26**, 3016 (1982).
[22]N. H. Tran, R. Kachru, P. Pillet, and T. F. Gallagher (unpublished).
[23]C. N. Yang, Phys. Rev. **74**, 764 (1948).
[24]W. Sandner, R. Kachru, K. A. Safinya, F. Gounand, W. E. Cooke, and T. F. Gallagher, Phys. Rev. A **27**, 1717 (1983).
[25]J. A. R. Samson and J. L. Gardner, Phys. Rev. Lett. **31**, 1327 (1973).
[26]We note that one must be careful about the significance of the Lu-Fano–type plot of the autoionizing state when more than two channels are involved. The Lu-Fano plot in this case is a two-dimensional projection of a higher-dimensional surface characterizing the position and widths of the state. See Ref. 14 for a detailed discussion.
[27]U. Fano and D. Dill, Phys. Rev. A **6**, 185 (1972).
[28]D. Dill and U. Fano, Phys. Rev. Lett. **29**, 1203 (1972).
[29]D. Dill, Phys. Rev. A **7**, 1976 (1973).
[30]J. Cooper and R. N. Zare, *Lectures in Theoretical Physics: Atomic Collision Processes* (Gordon and Breach, New York, 1969).
[31]This can be inferred by examining Eq. (17). If only $S^{(1)}$ were nonzero, then β(Ba II$6s_{1/2}$)$=-1$, which is a signature of parity-unfavored transitions. See Ref. 28.